

Single-well moment tensor inversion of tensile microseismic events

Vladimir Grechka¹, Zhao Li², Bo Howell², and Václav Vavryčuk³

ABSTRACT

Microseismic data acquired in a single observation well parallel to the axis of rotational symmetry of surrounding rocks — typically, in a vertical well drilled through a horizontally layered isotropic or vertically transversely isotropic formation — cannot be uniquely inverted for six independent components comprising the full seismic moment tensor. To constrain the inversion for such a survey geometry and medium symmetry, one might assume certain physical properties of seismic sources, the properties relating otherwise independent moment components to each other, regularizing moment tensor inversion, and helping reduce its ambiguity. Our paper examines one possibility of this kind: the assumption of a tensile fracture, rupturing the focal region along a plane of its greatest weakness. Mathematical formulation of inversion of single-well microseismic records for the parameters of tensile fractures reveals that the true solution, always recoverable from properly acquired data, might be accompanied by two spurious solutions. The analysis of those solutions leads to a criterion that, although not perfect, makes it possible to select the correct solution for the majority of elastic models. After being tested on synthetic, our methodology is applied to a field data set recorded with multiple vertical downhole arrays, demonstrating that the results of dual-well moment tensor inversion can be replicated with single-well data.

INTRODUCTION

Moment tensors estimated from microseismic data recorded to monitor hydraulic-fracturing operations usefully complement the event hypocenters, a standard deliverable of microseismic surveys. Even though computing moment tensors is more difficult, labori-

ous, and noise prone, than computing event hypocenters, practitioners are willing to undertake the task to find out details of the rupture process, helping them better understand the geomechanical behavior of unconventional reservoirs during their stimulation and production (e.g., Baig and Urbancic, 2010; Dohmen et al., 2014; Yang and Zoback, 2014; Staněk et al., 2015).

Inversion of full moment tensors \mathbf{M} , quantified by six independent components (e.g., Aki and Richards, 2002; Shearer, 2009), a well-posed problem with surface microseismic data often exhibiting beach ball-looking amplitude distributions for high-quality events (e.g., Eisner et al., 2010; Diller et al., 2015), is challenging with data acquired by borehole arrays, their narrow-angle, irregular directional apertures can lead to instabilities in the estimated moment components and even to ambiguity in moment tensor inversion (MTI). One particular example of this ambiguity — MTI of data collected by a vertical receiver array placed in a horizontally layered isotropic or vertically transversely isotropic (VTI) medium — is well documented in the literature (e.g., Nolen-Hoeksema and Ruff, 2001; Vavryčuk, 2007; Baig and Urbancic, 2010; Eaton and Forouhideh, 2011; Song and Toksöz, 2011; Rodriguez et al., 2011; Staněk and Eisner, 2013). In attempt to overcome the ambiguity, several authors (Rutledge and Phillips, 2003; Rutledge et al., 2013; Lee et al., 2014; Vavryčuk, 2015a; Yu et al., 2015, 2016) propose to compute the so-called “composite focal mechanisms” or “composite moment tensors” from data provided by a number of microseismic events that have similar waveforms. Their approach, although incapable of resolving individual focal mechanisms and moment tensors, yields an improved estimate of the composite, averaged over the selected events, moment tensor.

An alternative, preserving the ability to estimate tensors \mathbf{M} for individual microseismic events, lays in imposing certain physical characteristics on seismic sources. Just as the composite MTI approach regularizes the inversion by widening data aperture through combining the apertures of individual events, restricting the type of estimated focal mechanisms seeks to regularize MTI by establishing physically meaningful relationship or relationships

Manuscript received by the Editor 6 April 2016; revised manuscript received 5 July 2016; published online 29 September 2016.

¹Marathon Oil Company, Houston, Texas, USA. E-mail: vgrechka@marathonoil.com, grechkav@gmail.com.

²Borehole Seismic, LLC, Houston, Texas, USA. E-mail: zhao@boreholeseismic.co; bo.howell@boreholeseismic.com.

³Institute of Geophysics, Prague, Czech Republic. E-mail: vv@ig.cas.cz.

© 2016 Society of Exploration Geophysicists. All rights reserved.

between otherwise independent components of \mathbf{M} . Perhaps the most popular constraint of this type, sometimes borrowed by contemporary microseismic from the global seismology, is the assumption of a double-couple (DC) seismic source. Evidence collected from various hydraulic-fracturing jobs, however, suggests DC sources to be too restrictive (Jechumtálová and Eisner, 2008; Šílený et al., 2009; Kuehn et al., 2009) and implies a need for a more general source model than the DC model. Such a model, known as the tensile earthquake or the tensile seismic source, was proposed by Dufumier and Rivera (1997) and extended by Vavryčuk (2001, 2005, 2011).

In contrast to pure shear faulting described by DC sources, in which the slip or the displacement-discontinuity vector is confined to the fault or fracture plane, slips in tensile sources are oriented arbitrarily, predicting the existence of appreciable non-DC components in focal mechanisms of earthquakes and microseismic events (Vavryčuk, 2011, and references therein). The only assumption involved in the tensile-source model, the assumption shared with the double-couple model, is that rupture takes place at a planar fault or fracture. Physically, rupture of a focal region along a single plane of its greatest weakness is reminiscent of common observation of a chain breaking under tension at its weakest link rather than at several links simultaneously. Mathematically, the tensile-source model establishes a relationship between six generally independent moment components, helping constrain MTI of multi-well microseismic data and making MTI of single-well data almost unique for practical purposes.

In what follows, we review the theory of tensile seismic sources, explain how and in what way they regularize single-well MTI, and apply our findings to a downhole data set acquired in the Bakken Field (North Dakota, USA) with multiple observation wells. Comparison of full moment tensors estimated from data recorded in two wells with those estimated from data recorded in a single well shows that single-well MTI of tensile microseismic events is demonstratively feasible.

MOMENT AND SOURCE TENSORS OF TENSILE SEISMIC EVENTS

Consider a sudden slip at a planar fracture depicted in Figure 1. Such a seismic source has moment tensor \mathbf{M} with components (Aki

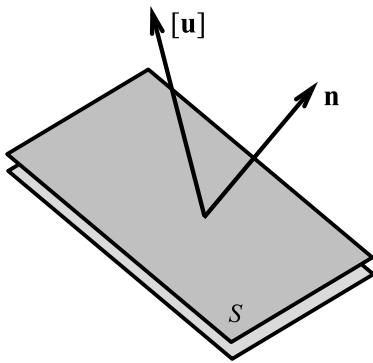


Figure 1. Slip $[\mathbf{u}]$ occurring over area S of a planar fracture that has unit normal \mathbf{n} . The angle between vector $[\mathbf{u}]$ and the fracture plane is defined as the slope (Vavryčuk, 2011).

and Richards, 2002, their equation 3.19 integrated over the focal volume)

$$M_{ij} = S c_{ijkl} [u_k] n_\ell, \quad (i, j = 1, 2, 3), \quad (1)$$

where S is the ruptured area, c_{ijkl} are the components of the fourth-rank stiffness tensor \mathbf{c} at the focal region, $[u_k]$ are the components of the slip vector $[\mathbf{u}]$, also termed the displacement-discontinuity vector or the displacement-dislocation vector (e.g., Ben-Menahem and Singh, 1981; Aki and Richards, 2002; Udías et al., 2014), and n_ℓ are the components of the unit normal \mathbf{n} to the fracture plane. In equation 1 and henceforth, Einstein summation from 1 to 3 with respect to all repeated low-case roman indexes, e.g., indexes k and ℓ , is assumed.

The symmetry of the stiffness tensor, yielding the relationship

$$c_{ijkl} [u_k] n_\ell = c_{ijk\ell} [u_\ell] n_k, \quad (i, j = 1, 2, 3), \quad (2)$$

allows us to rewrite equation 1 in its equivalent but more useful form (Ben-Menahem and Singh, 1981; Vavryčuk, 2005)

$$M_{ij} = c_{ijk\ell} D_{k\ell}, \quad (i, j = 1, 2, 3), \quad (3)$$

in which $D_{k\ell}$ are the components of symmetric, second-rank potency or source tensor \mathbf{D} defined as

$$D_{k\ell} \equiv \frac{1}{2} (b_k n_\ell + b_\ell n_k), \quad (k, \ell = 1, 2, 3), \quad (4)$$

with

$$b_k = S [u_k], \quad (k = 1, 2, 3). \quad (5)$$

Since directions of vectors \mathbf{b} and \mathbf{n} are assumed arbitrary, tensor \mathbf{D} contains a combination of pure shear (the component of $\mathbf{b} \perp \mathbf{n}$) and pure tensile (the component of $\mathbf{b} \parallel \mathbf{n}$) motions at a ruptured fracture; seismic sources described by tensor 4 are called the tensile sources (Vavryčuk, 2005, 2011).

Tensor \mathbf{D} , known as doublet in mathematics (Dattorro, 2005), has two unique properties: its determinant is zero,

$$\det \mathbf{D} = 0, \quad (6)$$

and the length $|\mathbf{b}|$ as well as the directions of vectors \mathbf{b} and \mathbf{n} are expressible through eigenvectors and nonzero eigenvalues of \mathbf{D} . Although the exact formulae for vectors \mathbf{b} and \mathbf{n} (found in Dattorro, 2005, his appendix B.2; and in Vavryčuk, 2005, 2011) are not important for our discussion, we mention the obvious ambiguity in characterizing tensile seismic sources given by two pairs of replacements,

$$\begin{cases} \mathbf{b} \rightarrow \mathbf{n}|\mathbf{b}|, \\ \mathbf{n} \rightarrow \frac{\mathbf{b}}{|\mathbf{b}|} \end{cases}, \quad (7)$$

and

$$\begin{cases} \mathbf{b} \rightarrow -\mathbf{b}, \\ \mathbf{n} \rightarrow -\mathbf{n}, \end{cases} \quad (8)$$

that leave tensor \mathbf{D} intact. Because of nonuniqueness in computing \mathbf{b} and \mathbf{n} , we deem a tensile source defined once its tensor \mathbf{D} is obtained.

Let us revisit equation 3 and, recognizing positive definiteness of tensor \mathbf{c} , invert the equation. The result,

$$D_{k\ell} = s_{k\ell ij} M_{ij}, \quad (k, \ell = 1, 2, 3), \quad (9)$$

where $\mathbf{s} = \mathbf{c}^{-1}$ denotes the compliance tensor of the focal region, is the recipe for computing \mathbf{D} from \mathbf{M} , provided that \mathbf{s} is known.

Next, we examine how parameters of tensile seismic sources — their tensors \mathbf{D} and \mathbf{M} — might be estimated from seismic data collected in a single straight well.

CHARACTERIZATION OF TENSILE SOURCES FROM SEISMIC DATA

Even though limitations imposed by single-well data-recording geometry on the estimation of moment tensors are known (Vavryčuk, 2007), we offer their brief review prior to discussing a remedy brought by our assumption of tensile seismic sources. The origin of nonuniqueness of MTI in such a geometry can be understood with the zeroth-order ray theory (e.g., Červený, 2001; Chapman, 2004); its generic expression for the amplitude of far-field displacement vector $\mathbf{d}(\mathbf{X})$ of a body wave recorded by a receiver located at \mathbf{X} has the form (e.g., Červený, 2001; Chapman, 2004)

$$\mathbf{d}(\mathbf{X}) = A\mathbf{U}(\mathbf{X})R. \quad (10)$$

Here A is the scalar amplitude factor accounting for geometrical spreading and transmission losses, $\mathbf{U}(\mathbf{X})$ is the unit polarization vector of a specified body wave (for instance, P- or S-wave) at the receiver, and R is the scalar source radiation pattern given by

$$R = p_i(\boldsymbol{\xi})M_{ij}U_j(\boldsymbol{\xi}), \quad (11)$$

where $p_i(\boldsymbol{\xi})$ and $U_j(\boldsymbol{\xi})$ are the components of the slowness vector $\mathbf{p}(\boldsymbol{\xi})$ and the unit polarization vector $\mathbf{U}(\boldsymbol{\xi})$, respectively, of wave excited at the source location $\boldsymbol{\xi}$.

Insight into ambiguity of the inversion, as it turns out, can be gained just by analyzing equation 11 (see Vavryčuk, 2007, for detail) rewritten as

$$R = \begin{bmatrix} M_{11} \\ M_{12} \\ M_{13} \\ M_{22} \\ M_{23} \\ M_{33} \end{bmatrix} \cdot \begin{bmatrix} p_1 U_1 \\ p_2 U_1 + p_1 U_2 \\ p_3 U_1 + p_1 U_3 \\ p_2 U_2 \\ p_3 U_2 + p_2 U_3 \\ p_3 U_3 \end{bmatrix}, \quad (12)$$

where the dot denotes the standard dot product and dependencies of the components of \mathbf{p} and \mathbf{U} on $\boldsymbol{\xi}$ are suppressed for brevity. When receivers compose a straight array, an appropriate coordinate transformation produces the geometry displayed in Figure 2, in which the receiver array (the triangles) is vertical, and the source is placed in the $[x_1, x_3]$ plane. For horizontally layered isotropic or VTI media, the ray trajectories in Figure 2 are confined to the $[x_1, x_3]$ plane, zeroing off-plane slowness components p_2 , reducing equation 12 to

$$R = \begin{bmatrix} M_{11} \\ M_{12} \\ M_{13} \\ M_{22} \\ M_{23} \\ M_{33} \end{bmatrix} \cdot \begin{bmatrix} p_1 U_1 \\ p_1 U_2 \\ p_3 U_1 + p_1 U_3 \\ 0 \\ p_3 U_2 \\ p_3 U_3 \end{bmatrix}, \quad (13)$$

and indicating that the moment component M_{22} is unrecoverable from data \mathbf{d} (equation 10) because the value of M_{22} does not influence R (equation 13). Alternatively, the absence of rotational symmetry with respect to the receiver array, either due to lateral velocity heterogeneity or azimuthal anisotropy, yields generally nonzero p_2 and can lead to unique and robust MTI of single-well data (Grechka, 2015).

Here we are interested in investigating full MTI of tensile microseismic events in the presence of rotational symmetry, that is, when the source radiation pattern is given by equation 13. Then, the five moment components — M_{11} , M_{12} , M_{13} , M_{23} , and M_{33} — are notionally invertible from data containing records of waves polarized vertically (P- and/or SV-waves) and horizontally (SH-waves); hence, the full moment tensor $\mathbf{M} = \mathbf{M}(M_{22})$ might be treated as a function of its yet unknown component M_{22} . This logic supposedly prompted Jechumtálová and Eisner (2008) to examine moment tensors $\mathbf{M}(M_{22})$ for a range of M_{22} values and find $\mathbf{M}(M_{22})$ to encompass vastly different focal mechanisms, essentially pointing to limited usefulness of single-well microseismic data for the characterization of seismic sources.

We, rather than vary the component M_{22} , choose to constrain it. Indeed, equation 9,

$$D_{ij}(M_{22}) = s_{ijk\ell} M_{k\ell}, \quad (i, j = 1, 2, 3), \quad (14)$$

makes source tensor \mathbf{D} a function of M_{22} , whereas equation 6,

$$\det \mathbf{D}(M_{22}) \equiv \det(s_{ijk\ell} M_{k\ell} |_{M_{22}=0} + s_{ij}^{(2)} M_{22}) = 0, \quad (15)$$

provides the relationship for computing M_{22} for a tensile microseismic event. The elements $s_{ij}^{(2)}$ of symmetric matrix $\mathbf{s}^{(2)}$, generally given as

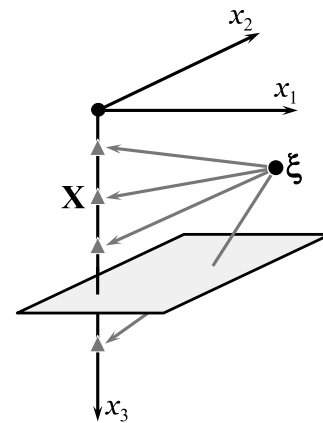


Figure 2. Rays (the gray lines with arrows) arriving from a source at $\boldsymbol{\xi}$ (the dot) to receivers (the gray triangles) placed in a vertical well.

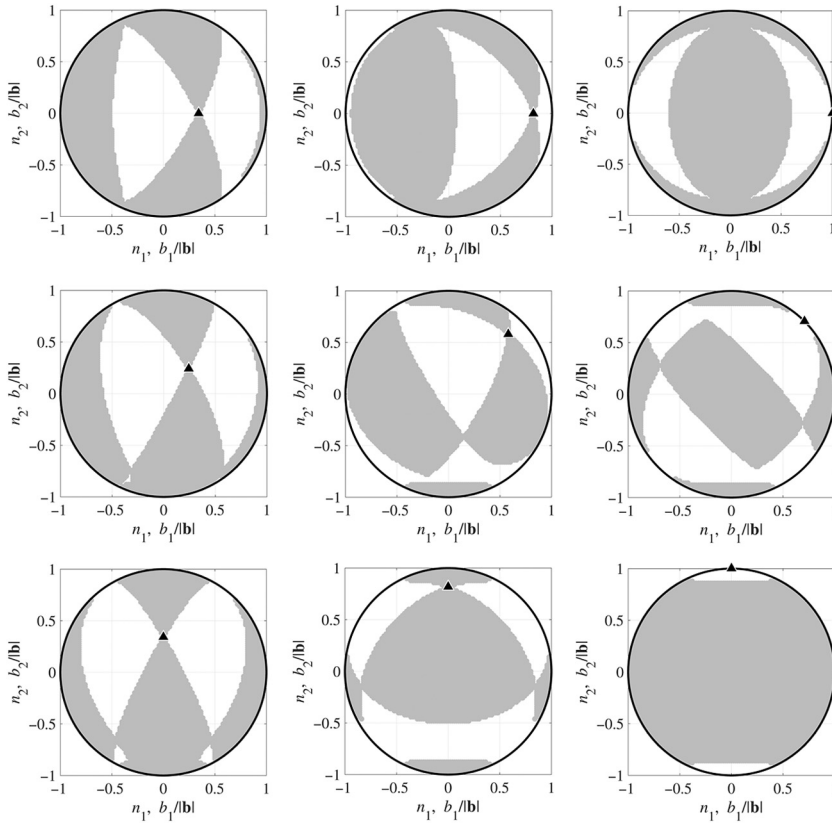


Figure 3. Stereographic projections at the lower unit hemisphere of vectors $\mathbf{b}/|\mathbf{b}|$, $b_3 \geq 0$ (gray) and \mathbf{n} (the black triangle) for which the true tensile source is recovered with algorithm 17. Selecting the vertical component $b_3 \leq 0$ reflects the displayed projections with respect to the coordinate origin.

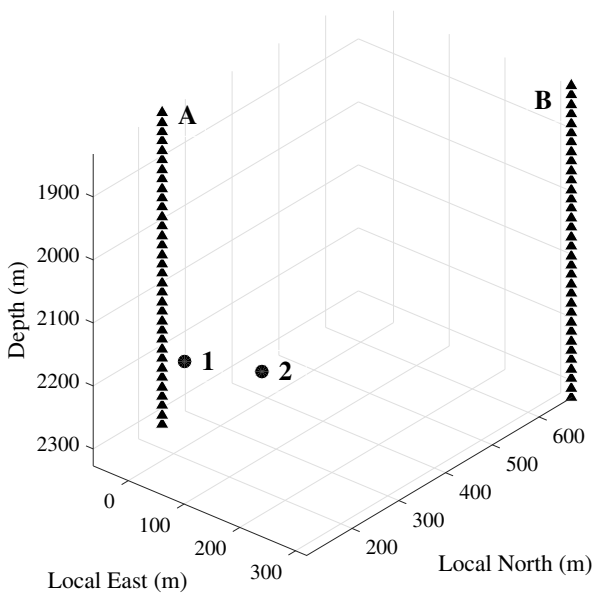


Figure 4. Geometry of synthetic data set. The triangles and circles mark locations of the receivers in wells A and B, and microseismic events 1 and 2, respectively.

$$\mathbf{s}^{(2)} = \begin{pmatrix} s_{12} & s_{26} & s_{25} \\ & s_{22} & s_{24} \\ & & s_{23} \end{pmatrix}, \quad (16)$$

make matrix $\mathbf{s}^{(2)}$ diagonal in isotropic and VTI media.

Equation 15, a cubic polynomial in M_{22} with real-valued coefficients, can have one or three real-valued roots potentially corresponding to M_{22} . If it has a single real-valued root, the desired solution for M_{22} is found; conversely, if all three roots of equation 15 are real-valued, a proper root has to be chosen.

Selection of root M_{22}

Since, as shown in Appendix A, the existence of three real-valued roots is plausible, we carried out numerical study, for various elastic parameters of the focal region and various tensile sources, to find out whether a formal mathematical criterion for selecting the correct value of M_{22} could be proposed. Our analysis indicates that the minimum by absolute value root yields the correct solution most of the time, leading to an algorithm:

select real-valued root M_{22} of equation 15 that has $\min |M_{22}|$. (17)

Criterion 17 is a regularization of sorts — if it fails to find the correct root, at least it selects the smallest root among those available, preventing tensors \mathbf{M} and \mathbf{D} from growing unjustifiably large.

Figure 3 illustrates the performance of our algorithm for VTI model of the focal region characterized by Thomsen (1986) parameters

$$\begin{aligned} V_{P0} &= 5.55 \text{ km/s}, & V_{S0} &= 3.00 \text{ km/s}, & \epsilon &= 0.09, \\ \delta &= 0.06, & \text{and } \gamma &= 0.10 \end{aligned} \quad (18)$$

that will be used in our synthetic example and field case study below. For a selected fracture normal \mathbf{n} (the black triangle), we scan over directions of vector \mathbf{b} on a grid with an increment of 0.01π radian and mark $\mathbf{b}/|\mathbf{b}|$ with a gray dot if algorithm 17 succeeds in finding the correct M_{22} for it. Depending on the direction of \mathbf{n} , the gray areas in different panels in Figure 3 vary in size, cumulatively covering 60% of tensile sources in this particular test and indicating the sources for which algorithm 17 works correctly. Effectiveness of the algorithm is found to depend most directly on the V_S/V_P ratio for isotropy and the V_{S0}/V_{P0} ratio for VTI media: The greater are the ratios, the higher is the success rate. For example, our algorithm finds the correct M_{22} for approximately 81% of tensile sources in a purely isotropic model that has $V_P = 4.5$ km/s and $V_S = 3.0$ km/s (not shown).

Still, information contained in equation 15 is clearly insufficient to ensure the correct selection of root M_{22} even for high V_S/V_P or V_{S0}/V_{P0} ratios. This deficiency is likely to be overcome with addi-

tional information normally available in field-data applications; for instance, the knowledge of reservoir geology or its geomechanical conditions might place certain restrictions on the types of expected moment tensors. We will postpone a survey of this extra information to the Discussion section and now turn our attention to examining MTI of tensile events on synthetic data.

SYNTHETIC DATA EXAMPLE

The model and results presented in Figures 4 and 5 are geared towards facilitating our forthcoming Bakken case study. Specifically, the receiver geometry in wells A and B in Figure 4 (the triangles) is close to that in Figure 6 below, the locations of events 1 and 2 in Figure 4 (the circles) correspond to the eastern and western edges of the cloud marked with the arrow in Figure 6, and homogeneous VTI model given by equation 18 has been estimated for the Lodgepole formation from field microseismic data.

We apply the dynamic ray tracing (e.g., Červený, 2001; Chapman, 2004) to compute amplitudes of the direct P- and SH-waves for two tensile events, their true source and moment tensors plotted in Figure 5a and 5e, respectively, and listed in Table 1. Event 1, an intentionally constructed double couple, maps itself exactly at the center of Hudson plot (Hudson et al., 1989) in Figure 5d (the circle), whereas event 2, having, also intentionally, a non-negligible tensile component is not in the center (another circle in Figure 5d). Note that tensor \mathbf{M} of the DC event does not fall into the center of Hudson plot in Figure 5h because anisotropy creates non-DC components of \mathbf{M} (Table 1), shifting the blue circle in Figure 5h away from the center of the plot, even though the corresponding tensor \mathbf{D} describes a pure double couple (see Šílený and Vavryčuk, 2002; Vavryčuk, 2005, 2006; and Leaney and Chapman, 2010, for discussion and further details). Anisotropy is also the cause for misalignments of eigenvectors of \mathbf{M} and \mathbf{D} ; they are not large enough to be clearly visible in the beach balls in Figure 5 (owing to small magnitudes of anisotropy coefficients ϵ , δ , and γ in equation 18) but responsible for differences in the strike, dip, rake, and slope angles of tensors \mathbf{M} and \mathbf{D} in Table 1.

To test the stability of single-well MTI, we contaminate the ray-traced amplitudes with Gaussian noise that has signal-to-noise ratio equal to 3, similar to that observed for the P-wave recorded in well B in our field data set (Figure 7 below), and apply the following inversion algorithm:

- select event data recorded in either well A or B;

- rotate the data and the model around the well to place the event in the $[x_1, x_3]$ plane of new coordinate frame, such as the one in Figure 2;
- compute five moment components M_{11} , M_{12} , M_{13} , M_{23} , and M_{33} by inverting equations 10 and 11;
- solve equation 15 for M_{22} and choose the real-valued root in accordance with criterion 17;
- rotate the obtained tensors \mathbf{M} and \mathbf{D} , the latter computed with equation 9, back to the original coordinate frame.

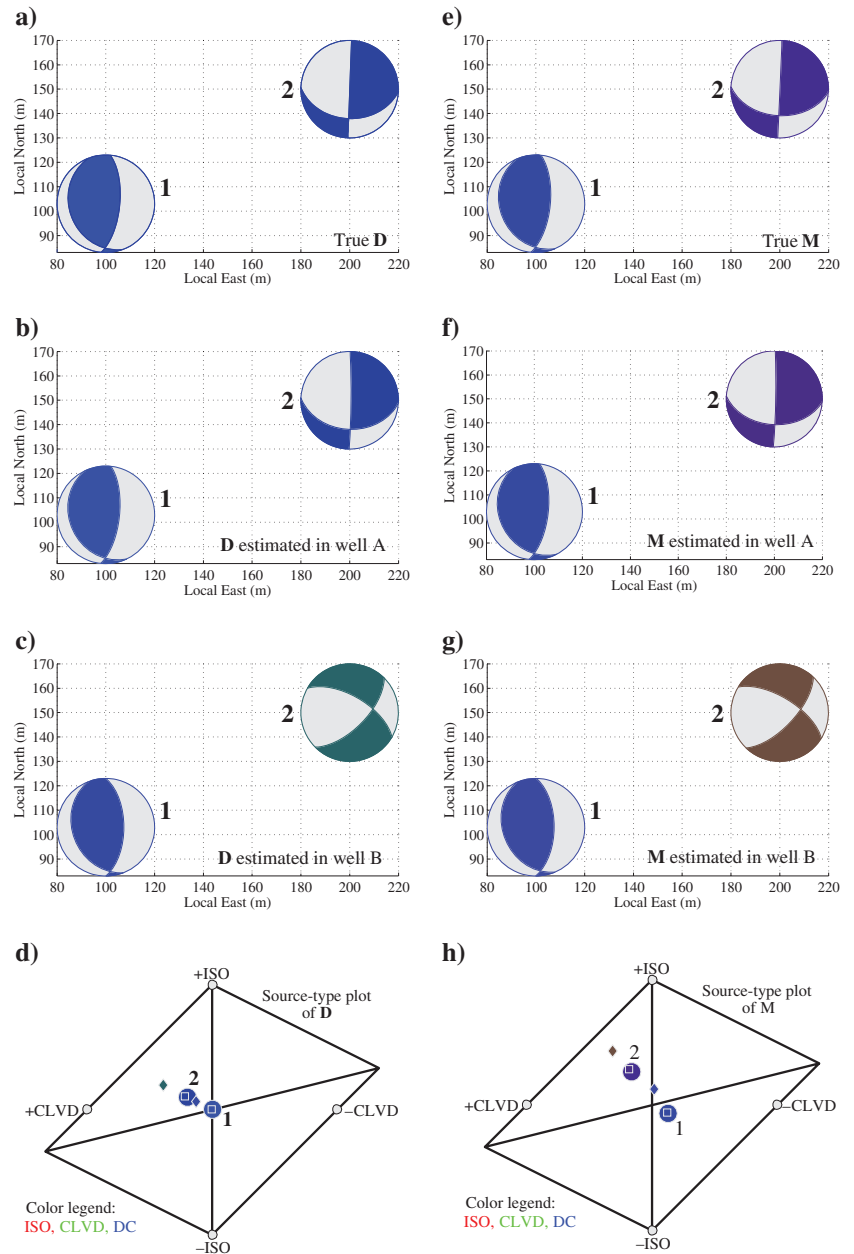


Figure 5. True (a) \mathbf{D} and (e) \mathbf{M} tensors, their inversion with data in (b), (f) well A and (c), (g) well B, and Hudson plots indicating the true (circles) and inverted (squares for well A and diamonds for well B) focal mechanisms of tensors (d) \mathbf{D} and (h) \mathbf{M} . The color legend for focal mechanisms in (d) and (h) is the same in all displays; the colors are mixed to reflect the fractions of the mechanisms. The beach balls in (a)–(c) and (e)–(g) represent the DC components of \mathbf{D} and \mathbf{M} . The event numbers 1 and 2 correspond to those in Figure 4.

Figure 5b and 5f displays tensors **D** and **M** estimated from data in well A (see Figure 4), at the lateral distance of approximately 250 m from the events. The estimates are accurate both in the percentages

of focal mechanisms (see Vavryčuk, 2001, on decomposition of tensors **M** and **D**), as evidenced by the squares mapped inside the circles in Figure 5d and 5h, and in the directions of nodal planes of their DC components (compare Figure 5a with 5b, Figure 5e with 5f, and the corresponding rows in Table 1). Inversion of data in well B, at the lateral distance of approximately 600 m from the events, is not as successful, as indicated by the beach balls in Figure 5c and 5g, by the diamonds shifting outside their respective circles in Figure 5d and 5h, and by the data misfits in Table 2. This time, particularly for non-DC event 2, an incorrect mixture of focal mechanisms and incorrect directions of nodal planes of its DC component (compare the upper-right beach balls in Figure 5a and 5c and Figure 5e and 5g) have been obtained. The reason for errors is noise; it is especially harmful for MTI of event 2 from data recorded in well B because unfavorably oriented focal mechanism of the event yields a weak signal in well B, more susceptible to noise than relatively stronger signal of event 1. Noise propagation into the estimates, quantified by condition numbers or, equivalently, by the ratios of maximum-to-minimum singular values (e.g., Press

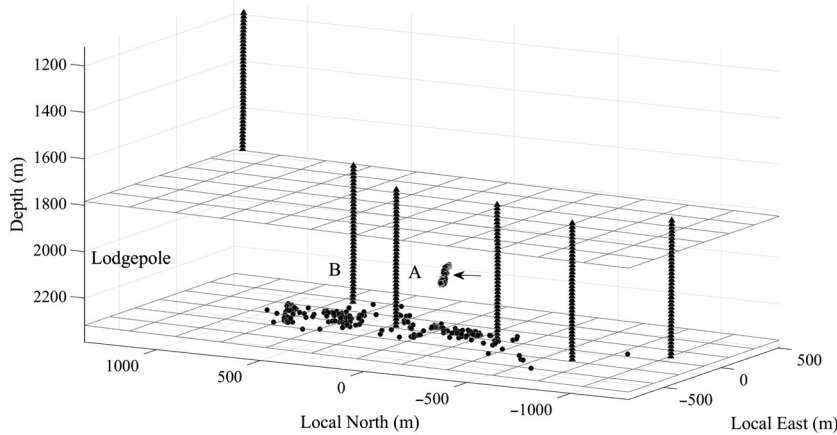


Figure 6. Microseismic recording geometry (the triangles in six nearly vertical wells), events (the dots) used to construct a layered anisotropic velocity model, and top and bottom of the Lodgepole formation (the planes dipping at 0.85° from north to south). Data collected by receivers placed in wells A and B are used to estimate moment tensors of microseismic events comprising a cloud marked with the arrow.

Table 1. Moment and source tensors in synthetic example. The components of **D are given in cm^3 , the components of **M** are in 0.1 MJ, and the fractions of focal mechanisms f_{ISO} , f_{CLVD} , f_{DC} of tensors **M** and **D** are dimensionless (see Vavryčuk, 2001, for their definitions). The strike, dip, and rake angles, calculated from the double-couple components of tensors **M** and **D**, as well as the slope angles (Vavryčuk, 2011), are in degrees. The density of the model is 2.52 g/cm^3 .**

Tensor D	D_{11}	D_{12}	D_{13}	D_{22}	D_{32}	D_{33}	f_{ISO}	f_{CLVD}	f_{DC}	Strike	Dip	Rake	Slope
Event 1													
True	0.12	-0.45	0.60	-3.20	-2.85	3.08	0.00	0.00	1.00	5.5	66.6	101.0	0.0
Estimated													
Well A	0.16	-0.59	0.70	-3.20	-2.91	3.07	0.00	0.01	0.99	6.0	67.1	103.3	0.2
Well B	0.00	-0.09	0.63	-4.13	-2.65	5.26	0.06	0.13	0.89	0.0	59.6	101.1	6.0
Event 2													
True	0.08	1.98	0.18	0.71	2.44	0.32	0.10	0.20	0.70	2.1	89.8	-50.6	10.1
Estimated													
Well A	0.22	2.00	0.21	0.83	2.36	0.18	0.11	0.22	0.67	0.5	87.9	-49.9	11.5
Well B	13.57	-2.27	0.09	-3.07	2.84	-2.36	0.20	0.39	0.41	45.0	63.8	-148.7	24.5
Tensor M	M_{11}	M_{12}	M_{13}	M_{22}	M_{32}	M_{33}	f_{ISO}	f_{CLVD}	f_{DC}	Strike	Dip	Rake	Slope
Event 1													
True	0.05	-0.25	0.27	-1.75	-1.29	1.27	-0.06	-0.12	0.82	5.9	65.9	102.7	-5.9
Estimated													
Well A	0.09	-0.32	0.32	-1.74	-1.32	1.27	-0.06	-0.12	0.82	6.5	66.5	105.2	-5.6
Well B	0.42	-0.47	0.29	-1.85	-1.20	2.58	0.13	-0.02	0.85	0.5	59.3	102.5	-1.0
Event 2													
True	0.45	1.08	0.08	0.80	1.11	0.54	0.27	0.16	0.57	2.5	89.6	-45.3	10.2
Estimated													
Well A	0.57	1.09	0.09	0.90	1.07	0.53	0.29	0.18	0.53	1.2	87.7	-44.6	12.0
Well B	10.41	-1.23	0.04	1.34	1.29	2.01	0.43	0.31	0.26	43.5	66.1	-152.2	28.6

et al., 2003) of matrixes appearing in the inverse problems solved in step (c) above, reveals the condition numbers to be between 20 and 30 for well A, closest to the events, and between 80 and 100 for well B, supplying useful guidance for field data processing.

Overall, this and other (not shown) tests on synthetic indicate that full moment and source tensors of tensile events can be estimated from microseismic data recorded in a single well, provided that velocity model and event hypocenters are precise (both the exact model and hypocenters were used in our synthetic example), high-quality amplitudes of direct arrivals are available, and the condition numbers of MTI are sufficiently low.

FIELD CASE STUDY

Next, we proceed with the application of the discussed methodology to field microseismic. We choose a data set acquired in the Bakken Field (North Dakota, USA) with six nearly vertical observation wells (Figure 6) because its data-acquisition geometry is ideal for the comparison of multi-well and single-well MTI. Since various aspects of this data set have been covered in Yang et al. (2013), Li et al. (2014), Dohmen et al. (2014), Yang and Zoback (2014), and Grechka et al. (2016), we outline only our data-processing steps pertaining to MTI.

We select 359 high signal-to-noise ratio events, pick times of the direct P- and S-waves, and apply microseismic tomography (Grechka and Yaskevich, 2013; 2014) to locate the events (the dots in Figure 6) jointly with constructing a layered anisotropic velocity model containing a mixture of homogeneous isotropic, VTI, and orthorhombic layers. Our velocity model (not shown) fits traveltime picks of the selected events with the root-mean-square misfit of 1.3 ms, giving us confidence in the precision of event hypocenters. For the purpose of estimating moment tensors of 25 events (marked with the arrow in Figure 6) located in the Lodgepole layer from data recorded by the receivers placed in the Lodgepole, only parameters of the Lodgepole formation itself (equation 18) are relevant.

Because MTI of data collected in a single vertical well necessarily relies on amplitudes of horizontally polarized shear-waves (equation 13), we estimate the receiver orientations and rotate seismic traces to the geographic (east, north, down) coordinates. The data displayed in Figure 7 clearly exhibit direct P- and S-wave arrivals, whose amplitudes serve as input for MTI. Although the records in well B in Figure 7 indicate split shear-waves, the horizontally polarized S-waves (the red traces) arriving earlier than the vertically polarized S-waves (the blue traces) similar to the arrivals observed by Grechka and Yaskevich (2014, their Figures 3 and 4) in an adjacent area of the Bakken Field, amplitudes of the slow S-waves proved to be too noisy for their use in MTI.

Having constructed the velocity model, having located the events, and having picked the amplitudes of the P- and fast S-waves, we apply steps (a)–(e) of the algorithm described in the previous

section to invert data collected in either well A or B (see Figure 6) for tensors \mathbf{M} and \mathbf{D} of tensile events. Acting upon our observation of the deterioration of accuracy of estimated moment and source tensors with the increase of the condition number of single-well MTI, we disregard estimates whose condition numbers in step (c) exceed 30. As a result, 19 out of 25 single-well inversions survive for data recorded in well A (the beach balls in Figure 8a and 8d

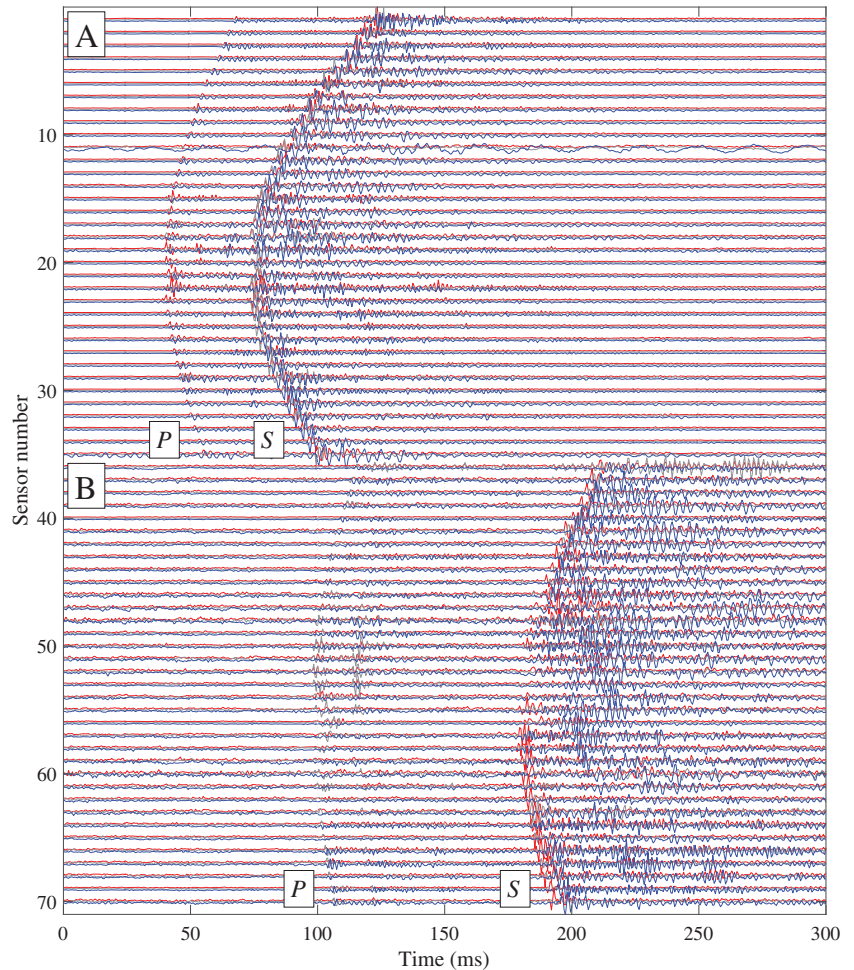


Figure 7. Typical three-component microseismic record by receivers placed inside the Lodgepole formation in wells A (the top 35 traces) and B (the bottom 35 traces) shown in Figure 6. The data are recorded with 0.5 ms sampling interval. The trace components are rotated to the east (red), north (gray), and down (blue).

Table 2. Data misfit $\|d - d^{\text{comp}}\|/\|d\|$ defined as ratio of the norm of the difference between noise-contaminated data d and data d^{comp} , computed with the estimated moment tensors in Table 1, and the norm of d itself.

	Data misfit	
	Event 1	Event 2
Well A	0.11	0.15
Well B	0.24	0.42

and the squares in Figure 8c and 8f), whereas none survives for data recorded in well B, the condition numbers ranging from 60 to 500 there.

The focal mechanisms displayed in Figure 8c and 8f imply the DC-dominated events accompanied by tensile fracture opening; the corresponding beach balls of the DC components of \mathbf{D} and \mathbf{M} (Figure 8a and 8d) indicate a mixture of normal and reverse faulting (with small strike-slip components) on steeply dipping fractures, whose orientation varies from N50°E at the eastern edge of the cloud (coinciding with the current maximum stress, S_{Hmax} , direction reported by Yang et al., 2013, and Yang and Zoback, 2014) to about N10°W at its western edge.

Next, we invert seismic data recorded in both wells A and B (Figure 6) for moment tensors of tensile events, that is, for the six components of \mathbf{M} constrained by equation 6. The results of dual-well MTI, displayed in Figure 8b, 8c, 8e, and 8f, confirm those obtained in our single-well inversion both for the focal mechanisms (compare the circles and squares in Figure 8c and 8f) and for the orientations of nodal planes of their DC components (compare Figure 8a with 8b and Figure 8d with 8e). The differences between the estimated moment and source tensors of individual events can be explained by noise in the data (Figure 7), influencing single-well MTI stronger than dual-well MTI because fewer amplitude picks are used in the

former than in the latter, and by inevitable inaccuracies in elastic parameters (given by equation 18) and event locations, propagating into tensors \mathbf{M} and \mathbf{D} through equations 9–11.

DISCUSSION

Our paper followed two threads:

- i) establishing mathematical formalism of the inversion of single-well microseismic data for moment tensors of tensile events, and
- ii) validating the formalism and the tensile-source model itself with field data.

We discuss those two lines of inquiry in turn.

Definition of tensile source tensor \mathbf{D} given by equation 4 reveals its key actionable property, $\det \mathbf{D} = 0$, constraining the moment components through equation 15. This equation might have two spurious roots for the moment component M_{22} (exemplified in Appendix A) that need to be computed and then discarded for the inversion to be successful. The main text proposes a formal criterion for the root selection; here we elaborate on other options that might be available for field data. Since typical MTI would be carried out for a collection of microseismic events rather than for a single event, and different M_{22} values entail pronounced differences in focal mechanisms (as noted by Jechumtálová and Eisner, 2008), requirement of internal consistency of the estimated moment tensors might be imposed, reducing the number of acceptable solutions by tying moment tensors of individual events to each other. Moreover, if equation 15 happens to have single real-valued roots M_{22} for some events, such as those for the majority of events in the low-right panel in Figure 3, uniquely computed M_{22} might serve as anchors for triple roots obtained for other events, shrinking the number of possibilities further. Additionally, physical constraints, such as more likely occurrence of nearly double couple focal mechanisms ($\mathbf{n} \sim \perp \mathbf{b}$, as those in Figure 8) than nearly tensile mechanisms ($\mathbf{n} \sim \parallel \mathbf{b}$), and geologic constraints, such as known stresses (see Vavryčuk, 2015b) or known faults in the area, could make some formal solutions improbable. All those options taken together lead us to believe that the problem of root selection should be tractable in practice, as was the case for our field data.

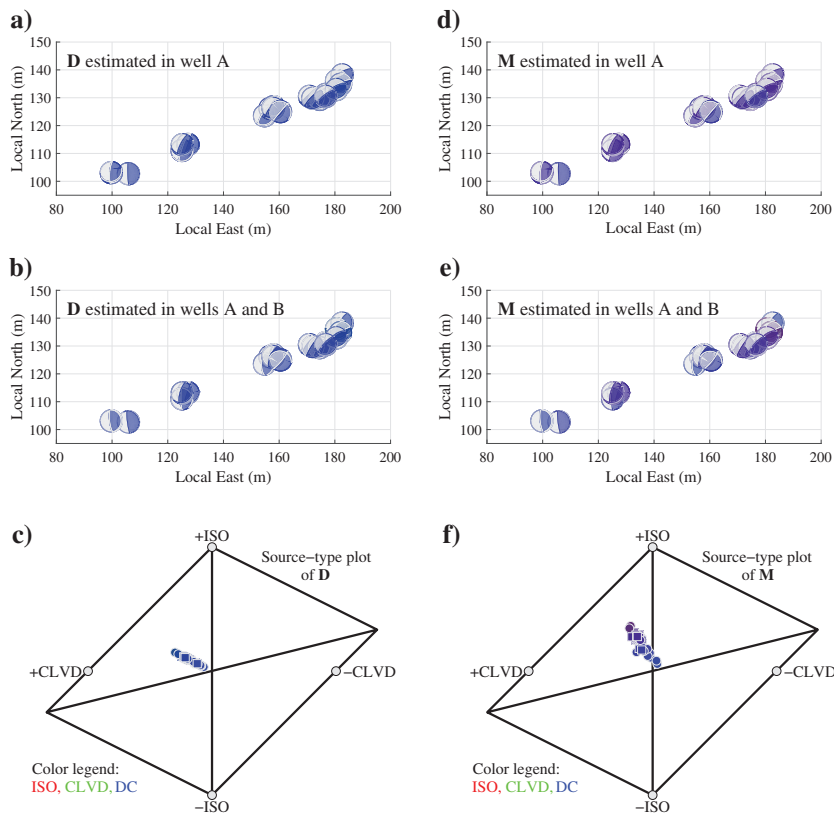


Figure 8. Tensors (a) \mathbf{D} and (d) \mathbf{M} computed from data collected in well A (in Figure 6) only, tensors (b) \mathbf{D} and (e) \mathbf{M} obtained from data recorded in both wells A and B, and Hudson plots displaying the values of (c) \mathbf{D} and (f) \mathbf{M} inverted from data in well A (squares) and in two wells (circles). The color legend for focal mechanisms in (c) and (f) is the same in all other panels. As in Figure 5, the mixtures of colors reflect the fractions of focal mechanisms, and the beach balls in (a), (b), (d), and (e) show the DC components of tensors \mathbf{D} and \mathbf{M} .

The choice of tensile-source model, primarily made because of the model's ability to describe both fracture opening, expected due to injection of fluids into a formation, and non-DC focal components observed in hydraulic-fracturing data sets (e.g., Zoback, 2007; Šílený et al., 2009; Baig and Urbancic, 2010; Fischer and Guest, 2011), was instrumental in regularizing MTI. Our more stable inversion procedure than general MTI, however, does not eliminate the need for careful data selection and processing. For example, we mentioned the removal of slow

shear-wave amplitudes from our inversion; we also excluded data recorded in the well immediately south from well A in Figure 6 (despite that well being closer to our event cloud than well B by about 100 m) because the data recorded there have generally lower signal-to-noise ratio than data recorded in wells A and B, making data from that well more harmful than helpful for MTI.

Having acknowledged our data-selection and data-processing choices, let us compare moment tensors in the eastern part of the cloud in Figure 8 with those presented in Figure 10c in Yang and Zoback (2014). The two papers clearly differ in event population, data that went into MTI (Yang and Zoback, 2014, used only the vertical components of the P-wave particle motions), and velocity models (isotropic in Yang and Zoback, 2014, with tops different from ours); and yet, the two beach ball displays are qualitatively similar, entailing the same interpretation of focal mechanisms as slips on steeply dipping fractures along and around the preexisting fault oriented at approximately N70°E. Quite curiously, the 60° rotation of nodal planes in Figure 8 (from about N50°E to N10°W) coincides with the angle between two conjugate faults in Figure 6c in Yang and Zoback (2014), providing circumstantial evidence that the fault hypothesized by Yang and Zoback (2014, the dashed red line in their Figure 6c) might actually exist. Geomechanical inferences made in the two papers are, however, different: many of our estimated moment tensors indicate reverse faulting, being suggestive of the relationship $S_V \lesssim S_{H \max}$ between the vertical, S_V , and maximum horizontal, $S_{H \max}$, stresses in the Lodgepole, whereas Yang and Zoback (2014), based on their MTI, conclude that $S_V \sim S_{H \max}$. The two statements, $S_V \lesssim S_{H \max}$ and $S_V \sim S_{H \max}$, not as contradictory as they might seem, could be reconciled if we take into account that our events are located above the depleted reservoir zone, where both stress regimes are possible (Ted Dohmen, personal communication). On the other hand, if the stress regime $S_V \lesssim S_{H \max}$ is, indeed, present, ambiguity between the slip and fracture-normal vectors expressed by replacements 7 makes our estimated focal mechanisms formally consistent with interpretation (proposed in Staněk and Eisner, 2013, and elaborated upon in Rutledge et al., 2015) of the events as slips induced by vertically growing hydraulic fractures at approximately horizontal bedding planes. Choosing one interpretation versus another requires additional geologic or geomechanical data that are not available at this time.

We conclude the paper by expressing our hope that single-well MTI of tensile events will be usefully applied for extracting more information from existing microseismic data sets and for planning new single-well microseismic surveys, armed with the knowledge that full moment tensors of recorded events can be estimated.

CONCLUSIONS

The goal of our paper has been to exploit the model of tensile seismic sources for stabilizing MTI of downhole microseismic data. After analyzing MTI of tensile events on synthetic, we tested it on field data, obtaining stable and internally consistent estimates corroborated by published moment tensors. Importantly and encouragingly for future applications, we have been able to demonstrate that focal mechanisms computed with dual-well and single-well input data are close to each other and entail the same interpretation.

The proposed criterion for choosing the value of the off-plane moment component for single-well MTI worked properly for both

our synthetic and field data, suggesting that mathematical issue of root selection is unlikely to have serious practical implications.

ACKNOWLEDGMENTS

We thank Marathon Oil Company for permission to publish the paper and Hess Corporation for providing the downhole data set. Václav Vavryčuk was partly supported by the Grant Agency of the Czech Republic, grants P210/12/1491 and 16-19751J. We are grateful to Ted Dohmen for his support and appreciate comments and suggestions received from Jan Šílený and an anonymous reviewer that helped us improve our paper.

APPENDIX A

EQUATION 15 FOR DOUBLE-COUPLE SOURCES IN ISOTROPIC MEDIA

The goal of this Appendix is to illustrate, with straightforward analytic examples, that equation 15 can have either one or three real-valued roots depending on the orientation of a ruptured fracture with respect to the recording array. To simplify our derivations, we assume isotropy of the focal region, its elastic properties described by the components of stiffness (e.g., Aki and Richards, 2002, their equation 2.33),

$$c_{ijk\ell}^{\text{ISO}} = \lambda \delta_{ij} \delta_{k\ell} + \mu (\delta_{ik} \delta_{j\ell} + \delta_{i\ell} \delta_{jk}), \quad (i, j, k, \ell = 1, 2, 3), \quad (\text{A-1})$$

or compliance,

$$s_{ijk\ell}^{\text{ISO}} = \frac{1}{4\mu} \left(\delta_{ik} \delta_{j\ell} + \delta_{i\ell} \delta_{jk} - \frac{2\lambda}{3K} \delta_{ij} \delta_{k\ell} \right), \quad (i, j, k, \ell = 1, 2, 3), \quad (\text{A-2})$$

tensors, where δ_{ij} is the Kronecker delta, λ and μ are the Lamé constants, and

$$K = \lambda + \frac{2}{3}\mu \quad (\text{A-3})$$

is the bulk modulus. Equations A-1 and A-2 reduce the general relationships 3 and 9 to

$$M_{ij} = \lambda D_{kk} \delta_{ij} + 2\mu D_{ij}, \quad (i, j = 1, 2, 3) \quad (\text{A-4})$$

and

$$D_{ij} = \frac{1}{2\mu} \left(M_{ij} - \frac{\lambda}{3K} M_{kk} \delta_{ij} \right), \quad (i, j = 1, 2, 3). \quad (\text{A-5})$$

Single real-valued root

We begin with a double-couple source defined by the fracture normal $\mathbf{n} = [0, 1, 0]$ and vector $\mathbf{b} = [0, 0, b_3]$. Its symmetric source tensor given by equation 4,

$$\mathbf{D} = \frac{1}{2} \begin{pmatrix} 0 & 0 & 0 \\ 0 & 0 & b_3 \\ 0 & 0 & 0 \end{pmatrix}, \quad (\text{A-6})$$

yields the symmetric moment tensor (see equation A-4)

$$\mathbf{M} = \mathbf{M}(M_{22}) = \begin{pmatrix} 0 & 0 & 0 \\ & M_{22} & \mu b_3 \\ & & 0 \end{pmatrix}, \quad (\text{A-7})$$

in which

$$M_{22} = 0. \quad (\text{A-8})$$

Substitution of tensor A-7 into equation 14 in its isotropic version A-5 results in source tensor

$$\begin{aligned} \mathbf{D}(M_{22}) &= \frac{1}{2\mu} \left[\begin{pmatrix} 0 & 0 & 0 \\ & M_{22} & \mu b_3 \\ & & 0 \end{pmatrix} \right. \\ &\quad \left. - \frac{\lambda}{3K} \begin{pmatrix} M_{22} & 0 & 0 \\ & M_{22} & 0 \\ & & M_{22} \end{pmatrix} \right] \\ &= \frac{1}{6\mu K} \begin{pmatrix} -\lambda M_{22} & 0 & 0 \\ & 2(\lambda + \mu)M_{22} & 3\mu K b_3 \\ & & -\lambda M_{22} \end{pmatrix} \quad (\text{A-9}) \end{aligned}$$

and in equation 15

$$\det \mathbf{D}(M_{22}) = \frac{\lambda M_{22}}{(6\mu K)^3} [2\lambda(\lambda + \mu)M_{22}^2 + (3\mu K b_3)^2] = 0 \quad (\text{A-10})$$

that has single real-valued root $M_{22} = 0$ for isotropic rocks with (typically) positive Lamé constant λ . Clearly, the true value of M_{22} given by equation A-8 has been recovered from equation A-10.

Three real-valued roots

Next, we keep the same vector $\mathbf{b} = [0, 0, b_3]$ and change the fracture normal from the previous example to $\mathbf{n} = [1, 0, 0]$. Equations A-6, A-7, A-9, and A-10 then take the form

$$\mathbf{D} = \frac{1}{2} \begin{pmatrix} 0 & 0 & b_3 \\ & 0 & 0 \\ & & 0 \end{pmatrix}, \quad (\text{A-11})$$

$$\mathbf{M} = \mathbf{M}(M_{22}) = \begin{pmatrix} 0 & 0 & \mu b_3 \\ & M_{22} & 0 \\ & & 0 \end{pmatrix}, \quad (\text{A-12})$$

$$\mathbf{D}(M_{22}) = \frac{1}{6\mu K} \begin{pmatrix} -\lambda M_{22} & 0 & 3\mu K b_3 \\ & 2(\lambda + \mu)M_{22} & 0 \\ & & -\lambda M_{22} \end{pmatrix}, \quad (\text{A-13})$$

and

$$\det \mathbf{D}(M_{22}) = \frac{2(\lambda + \mu)M_{22}}{(6\mu K)^3} [(\lambda M_{22})^2 - (3\mu K b_3)^2] = 0, \quad (\text{A-14})$$

respectively. This time, in addition to the correct root $M_{22} = 0$, equation A-14 contains two spurious real-valued roots

$$M_{22} = \pm \left| \frac{3\mu K b_3}{\lambda} \right|, \quad (\text{A-15})$$

implying the need for devising a root-selection criterion.

REFERENCES

- Aki, K., and P. G. Richards, 2002, Quantitative seismology, 2nd ed.: University Science Books.
- Baig, A., and T. Urbancic, 2010, Microseismic moment tensors: A path to understanding frac growth: *The Leading Edge*, **29**, 320–324, doi: [10.1190/1.3353729](https://doi.org/10.1190/1.3353729).
- Ben-Menahem, A., and S. J. Singh, 1981, Seismic waves and sources: Springer-Verlag.
- Červený, V., 2001, Seismic ray theory: Cambridge University Press.
- Chapman, C., 2004, Fundamentals of seismic wave propagation: Cambridge University Press.
- Dattorro, J., 2005, Convex optimization & Euclidean distance geometry: Meboo Publishing.
- Diller, D. E., T. Shuck, and B. Fish, 2015, Estimation and interpretation of high-confidence microseismic source mechanisms: *The Leading Edge*, **34**, 918–924, doi: [10.1190/le34080918.1](https://doi.org/10.1190/le34080918.1).
- Dohmen, T., J.-P. Blangy, and J. Zhang, 2014, Microseismic depletion delineation: Interpretation, **2**, SG1–SG13, doi: [10.1190/INT-2013-0164.1](https://doi.org/10.1190/INT-2013-0164.1).
- Dufumier, H., and L. Rivera, 1997, On the resolution of the isotropic component in moment tensor inversion: *Geophysical Journal International*, **131**, 595–606, doi: [10.1111/j.1365-246X.1997.tb06601.x](https://doi.org/10.1111/j.1365-246X.1997.tb06601.x).
- Eaton, D. W., and F. Forouhdeh, 2011, Solid angles and the impact of receiver-array geometry on microseismic moment-tensor inversion: *Geophysics*, **76**, no. 6, WC77–WC85, doi: [10.1190/geo2011-0077.1](https://doi.org/10.1190/geo2011-0077.1).
- Eisner, L., S. Williams-Stroud, A. Hill, P. Duncan, and M. Thornton, 2010, Beyond the dots in the box: Microseismicity-constrained fracture models for reservoir simulation: *The Leading Edge*, **29**, 326–333, doi: [10.1190/1.3353730](https://doi.org/10.1190/1.3353730).
- Fischer, T., and A. Guest, 2011, Shear and tensile earthquakes caused by fluid injection: *Geophysical Research Letters*, **38**, L05307, doi: [10.1029/2010GL045447](https://doi.org/10.1029/2010GL045447).
- Grechka, V., 2015, On the feasibility of inversion of single-well microseismic data for full moment tensor: *Geophysics*, **80**, no. 4, KS41–KS49, doi: [10.1190/geo2014-0471.1](https://doi.org/10.1190/geo2014-0471.1).
- Grechka, V., and S. Yaskevich, 2013, Inversion of microseismic data for triclinic velocity models: *Geophysical Prospecting*, **61**, 1159–1170, doi: [10.1111/1365-2478.12042](https://doi.org/10.1111/1365-2478.12042).
- Grechka, V., and S. Yaskevich, 2014, Azimuthal anisotropy in microseismic monitoring: A Bakken case study: *Geophysics*, **79**, no. 1, KS1–KS12, doi: [10.1190/geo2013-0211.1](https://doi.org/10.1190/geo2013-0211.1).
- Grechka, V., Z. Li, and B. Howell, 2016, Relative location of microseismic events with multiple masters: *Geophysics*, **81**, no. 4, KS149–KS158, doi: [10.1190/geo2015-0445.1](https://doi.org/10.1190/geo2015-0445.1).
- Hudson, J. A., R. G. Pearce, and R. M. Rogers, 1989, Source type plot for inversion of the moment tensor: *Journal of Geophysical Research*, **94**, 765–774, doi: [10.1029/JB094iB01p00765](https://doi.org/10.1029/JB094iB01p00765).
- Jechumtálová, Z., and L. Eisner, 2008, Seismic source mechanism inversion from a linear array of receivers reveals non-double-couple seismic events induced by hydraulic fracturing in sedimentary formation: *Tectonophysics*, **460**, 124–133, doi: [10.1016/j.tecto.2008.07.011](https://doi.org/10.1016/j.tecto.2008.07.011).
- Kuehn, D., H. N. Gharti, V. Oye, and M. Roth, 2009, Automatic determination of full moment tensor solutions from P-wave first motion amplitudes: EAGE Workshop on Passive Seismic, A05.
- Leaney, S., and C. Chapman, 2010, Microseismic sources in anisotropic media: 72nd Annual International Conference and Exhibition, EAGE, Extended Abstracts, F015.
- Lee, M., T. Davis, and S. Maxwell, 2014, The use of amplitude ratios to constrain source mechanisms of microseismic data: A case study from the Montney Shale, Alberta: *First Break*, **32**, 67–73.
- Li, J., C. Li, S. A. Morton, T. Dohmen, K. Katahara, and M. N. Toksöz, 2014, Microseismic joint location and anisotropic velocity inversion for hydraulic fracturing in a tight Bakken reservoir: *Geophysics*, **79**, no. 5, C111–C122, doi: [10.1190/geo2013-0345.1](https://doi.org/10.1190/geo2013-0345.1).

- Nolen-Hoeksema, R. C., and L. J. Ruff, 2001, Moment tensor inversion of microseisms from the B-sand propped hydrofracture, M-site, Colorado: *Tectonophysics*, **336**, 163–181, doi: [10.1016/S0040-1951\(01\)00100-7](https://doi.org/10.1016/S0040-1951(01)00100-7).
- Press, W. A., S. A. Teukolsky, W. T. Vetterlink, and B. P. Flannery, 2003, *Numerical recipes in Fortran 77: The art of scientific computing*: Cambridge University Press.
- Rodriguez, I. V., Y. J. Gu, and M. D. Sacchi, 2011, Resolution of seismic-moment tensor inversions from a single array of receivers: *Bulletin of the Seismological Society of America*, **101**, 2634–2642, doi: [10.1785/0120110016](https://doi.org/10.1785/0120110016).
- Rutledge, J., R. Downie, S. Maxwell, J. Drew, and T. Fischer, 2013, Extension-shear microseismic mechanisms during hydraulic fracturing: 83rd Annual International Meeting, SEG, Expanded Abstracts, 2067–2072.
- Rutledge, J. T., and W. S. Phillips, 2003, Hydraulic stimulation of natural fractures as revealed by induced microearthquakes, Carthage Cotton Valley gas field, east Texas: *Geophysics*, **68**, 441–452, doi: [10.1190/1.1567214](https://doi.org/10.1190/1.1567214).
- Rutledge, J., X. Yu, and S. Leaney, 2015, Microseismic shearing driven by hydraulic-fracture opening: An interpretation of source-mechanism trends: *The Leading Edge*, **34**, 926–934, doi: [10.1190/tle34080926.1](https://doi.org/10.1190/tle34080926.1).
- Shearer, M., 2009, *Introduction to seismology*, 2nd ed.: Cambridge University Press.
- Šílený, J., and V. Vavryčuk, 2002, Can unbiased source be retrieved from anisotropic waveforms by using an isotropic model of the medium?: *Tectonophysics*, **356**, 125–138, doi: [10.1016/S0040-1951\(02\)00380-3](https://doi.org/10.1016/S0040-1951(02)00380-3).
- Šílený, J., L. Eisner, D. P. Hill, and F. H. Cornet, 2009, Non-double-couple mechanisms of microearthquakes induced by hydraulic fracturing: *Journal of Geophysical Research*, **114**, B08307, doi: [10.1029/2008JB005987](https://doi.org/10.1029/2008JB005987).
- Song, F., and M. N. Toksöz, 2011, Full-waveform based complete moment tensor inversion and source parameter estimation from downhole microseismic data for hydrofracture monitoring: *Geophysics*, **76**, no. 6, WC103–WC116, doi: [10.1190/geo2011-0027.1](https://doi.org/10.1190/geo2011-0027.1).
- Staněk, F., and L. Eisner, 2013, New model explaining inverted source mechanisms of microseismic events induced by hydraulic fracturing: 83rd Annual International Meeting, SEG, Expanded Abstracts, 2201–2205, doi: [10.1190/segam2013-0554.1](https://doi.org/10.1190/segam2013-0554.1).
- Staněk, F., Z. Jechumtálová, and L. Eisner, 2015, Reservoir stress from microseismic source mechanisms: *The Leading Edge*, **34**, 890–895, doi: [10.1190/tle34080890.1](https://doi.org/10.1190/tle34080890.1).
- Thomsen, L., 1986, Weak elastic anisotropy: *Geophysics*, **51**, 1954–1966, doi: [10.1190/1.1442051](https://doi.org/10.1190/1.1442051).
- Udías, A., R. Madariaga, and E. Buforn, 2014, *Source mechanisms of earthquakes: Theory and practice*: Cambridge University Press.
- Vavryčuk, V., 2001, Inversion for parameters of tensile earthquakes: *Journal of Geophysical Research*, **106**, 16339–16355, doi: [10.1029/2001JB000372](https://doi.org/10.1029/2001JB000372).
- Vavryčuk, V., 2005, Focal mechanisms in anisotropic media: *Geophysical Journal International*, **161**, 334–346, doi: [10.1111/j.1365-246X.2005.02585.x](https://doi.org/10.1111/j.1365-246X.2005.02585.x).
- Vavryčuk, V., 2006, Focal mechanisms produced by shear faulting in weakly transversely isotropic crustal rocks: *Geophysics*, **71**, no. 5, D145–D151, doi: [10.1190/1.2236378](https://doi.org/10.1190/1.2236378).
- Vavryčuk, V., 2007, On the retrieval of moment tensors from borehole data: *Geophysical Prospecting*, **55**, 381–391, doi: [10.1111/j.1365-2478.2007.00624.x](https://doi.org/10.1111/j.1365-2478.2007.00624.x).
- Vavryčuk, V., 2011, Tensile earthquakes: Theory, modeling, and inversion: *Journal of Geophysical Research*, **116**, B12320, doi: [10.1029/2011JB008770](https://doi.org/10.1029/2011JB008770).
- Vavryčuk, V., 2015a, Inversion for the composite moment tensor: *Bulletin of the Seismological Society of America*, **105**, 3024–3035, doi: [10.1785/0120150163](https://doi.org/10.1785/0120150163).
- Vavryčuk, V., 2015b, Earthquake mechanisms and stress field, *in* M. Beer, I. A. Kougioumtzoglou, E. Patelli, and I. Siu-Kui Au, eds., *Encyclopedia of earthquake engineering*: Springer-Verlag, doi: [10.1007/978-3-642-36197-5_295-1](https://doi.org/10.1007/978-3-642-36197-5_295-1).
- Yang, Y., and M. D. Zoback, 2014, The role of preexisting fractures and faults during multistage hydraulic fracturing in the Bakken Formation: *Interpretation*, **2**, SG25–SG39, doi: [10.1190/INT-2013-0158.1](https://doi.org/10.1190/INT-2013-0158.1).
- Yang, Y., M. Zoback, M. Simon, and T. Dohmen, 2013, An integrated geo-mechanical and microseismic study of multi-well hydraulic fracture stimulation in the Bakken formation: Unconventional Resources Technology Conference, URTeC 1580301.
- Yu, X., J. Rutledge, and S. Leaney, 2015, Event grouping and multi-event moment-tensor inversion for ill-posed monitoring geometry: 85th Annual International Meeting, SEG, Expanded Abstracts, 2522–2526, doi: [10.1190/segam2015-5876354.1](https://doi.org/10.1190/segam2015-5876354.1).
- Yu, X., S. Leaney, J. Rutledge, and C. Chapman, 2016, Multievent moment-tensor inversion for ill-conditioned geometries: *Geophysics*, **81**, no. 2, KS11–KS24, doi: [10.1190/geo2015-0074.1](https://doi.org/10.1190/geo2015-0074.1).
- Zoback, M. D., 2007, *Reservoir geomechanics*: Cambridge University Press.